Quantitative MRI analysis of structural changes in tomato tissues resulting from dehydration

Rodolphe Leforestier, Anna Fleury, François Mariette, Guylaine G. Collewet, Sylvain Challois, Maja Musse

Quantitative MRI analysis of structural changes in tomato tissues resulting from dehydration

Authors: Rodolphe Leforestier, Anna Fleury, François Mariette, Guylaine Collewet, Sylvain Challois, Maja Musse*

Summary

A quantitative MRI analysis at 1.5T of the effects of different dehydration regimes on relaxation parameters measured in tomato tissue is presented. Multi-exponential T_2 maps have been estimated for the first time, providing access to spatialized microstructural information at voxel scale. The objective was to provide a better understanding of the changes in the multi-exponential transverse relaxation parameters induced by dehydration in tomato tissues and to unravel the effects of microstructure and composition on relaxation parameters.

The results led to the hypothesis that the multi-exponential relaxation signal reflects cell compartmentation and tissue heterogeneity, even at the voxel scale. Multi-exponential relaxation times provided information about water loss from specific cell compartments and seems to indicate that the dehydration process mainly affects large cells. By contrast, total signal intensity showed no sensitivity to variations in water content in the range investigated in the present study (between 95% (fresh tissue) and 90% (after dehydration)). The variation in relaxation times resulting from water loss was due to both changes in solute concentration and compartment size. The comparative analysis of the two contrasted tissues in terms of microporosity demonstrated that magnetic susceptibility effects, caused by the presence of air in the placenta tissue, significantly impacts the effective relaxation and might be the dominant effect in the variations observed in relaxation times in this tissue.

Introduction

The usefulness of Nuclear Magnetic Resonance (NMR) for obtaining information on water distribution and transfers in plant tissues during physiological or physical processes has been demonstrated in numerous studies [1-9]. Indeed, multi-exponential transverse relaxation reflects the behavior of water protons in different environments, allowing it therefore to provide information about subcellular water compartmentation in plant tissues. While a large number of these studies have been carried out using NMR, there is a growing body of work that adopts a similar approach using Magnetic Resonance Imaging (MRI) [10-18], thanks to the methodological advances made in recent years. Compared to NMR, the advantage of MRI Relaxometry is that it offers a non-invasive and spatially-resolved way to provide such quantitative information on relaxation times, along with macroscopic structural information.

Of the various physiological and technological transformations that occur, dehydration is one of the most investigated. Several NMR [2, 3, 19, 20] and MRI [13, 21-23] studies have been carried out on samples of different fruits and vegetables under various dehydration regimes. There are discrepancies in the outcomes in terms of T_2 and signal-intensity variations as a function of water loss, while the assumptions on which the authors base their interpretation of the data diverge. The discrepancies can be explained by the complexity of the relaxation mechanisms, which depend on the physical and chemical characteristics of the tissue and are affected by the acquisition conditions (temperature, magnetic field strength, relaxation signal sampling). Indeed, drying induces changes in the solute concentration of aqueous solutions contained in cell compartments, leading to variations in their bulk relaxation times via chemical exchange mechanisms [24, 25]. Drying also impacts self-diffusion coefficients, which display a linear decrease with solute concentration under a dilute regime [26]. Further, dehydration leads to significant changes in cell size and may induce alterations in membrane permeability [27, 28], thereby modifying diffusional exchanges of water molecules between cell compartments.

A current challenge is to arrive at a better understanding of the changes in the multi-exponential transverse relaxation parameters induced by the dehydration of plant tissues and to unravel the effects of microstructure and composition on relaxation parameters. This would make it possible to take full advantage of MRI for the further investigation of drying processes. Indeed, the dehydration of fruit and vegetables, which enables the activity of microbes and molds to be halted through the partial removal of water, is one of the most common and simple processes for their preservation. Dehydration leads to changes in both tissue microstructure and macroscopic characteristics. Although dehydration of fruit is a relatively well-studied process, there is a lack of information concerning the microstructural changes that occur during this process [29]. However, we do know that the preservation of water compartmentation along with changes in microporosity will generally affect the texture and the nutritional and digestive qualities of the dried product. Characterization of these parameters is therefore crucial for the understanding of drying mechanisms and to improve knowledge of final product properties.

This work therefore aims to study the variations in transverse relaxation signal during the dehydration process in tomato, considering both the effect of the water content and structural variations within the tissues. An MRI approach was employed [10, 30] for the estimation of the multi-T_2 relaxation parameters at the voxel scale. The study was performed on tomato, which offers a well-documented model where the tissues have different intrinsic microstructures in terms of cell size [31] and gas proportion [32], thereby providing an ideal subject for the purpose of the present study. The analyses focused on the equatorial pericarp and placenta, as these are the two tomato tissues that display the greatest contrast in term of porosity and cell sizes. The modulation of the kinetics and the amount of water loss has made it possible to analyze fruit tissues with similar water contents but obtained under different drying conditions. In order to experimentally determine the relationship between T_2 and the diffusion coefficient that follows the concentration of aqueous solutions, T_2 and the diffusion coefficient were measured in fructose solutions at a pH value of 4.4 (corresponding to that measured in tomato) in the

water content ranges expected for fresh and dried tomato tissues. In addition to the mapping of multi-exponential transverse relaxation, MRI was used to resolve morphological changes of tissues and to quantify their microporosity and water self-diffusion. The relationship of these parameters to changes in the water content of tissues was explored.

Experimental

Plant material

Ripe vine tomatoes of similar color and size were purchased from the local market. Four similar tomatoes from a truss were chosen for each dehydration experiment and four more tomatoes from the same truss were saved for associated destructive analyses. The experiments were carried out on slices 1.5 cm thick, cut in the equatorial region perpendicular to the pedicle axis. Before the MRI experiments, (fresh and dried) slices were wiped to remove any water released from the broken cells and were then individually wrapped in cling film to prevent water evaporation during image acquisition.

Experimental Design

Tomato experiment

A target was set of about 40% total mass loss per tomato slice to reduce the water content of the equatorial pericarp by a few percent while maintaining cell integrity. Cell integrity was verified in preliminary experiments by using light microscopy to observe pericarp samples before and after dehydration. To achieve a mass loss of about 40%, the tomato slices were placed on racks and were dehydrated in a cold room at 4°C for 7 days (regime 1-A), in a ventilated oven at 40°C for 9 hours (regime 2) and in a vacuum oven at 40°C and 50mbar for 23 hours (regime 3). An additional regime (1-B) consisted of the storage of the tomato slices in a cold room at 4°C for 5 days leading to a mass loss of about 30%, making it possible to compare tomato tissues processed using the same dehydration process but with different mass losses. The dehydration conditions are summarized in Table 1.

First, MRI analyses were performed on fresh tomato slices immediately after cutting. In each imaging experiment, four tomato slices were positioned on a base with a tube of aqueous manganese solution placed in the center to check the stability of the MRI measurements. After MRI analysis, the tomato slices were subjected to the dehydration protocol. In order to stabilize the tissues after dehydration and to minimize water content gradients within the tissues, the dehydrated slices were stored at 4°C overnight before being analyzed again by MRI. They were placed in the same position as in the first imaging experiment by following a recording protocol using sheets of graph paper and marks made on the slices.

Water content measurements were carried out on three cylindrical samples (diameter 1cm) taken from the equatorial pericarp and two from the placenta of each tomato slice. To estimate the water content of the fresh tissues, samples were taken from the central slices of the tomatoes allocated to destructive analysis. In this case, a single water content value per tomato was estimated. In the case of dried tissues, the samples were taken from the slices imaged by MRI. The positions of the samples (Figure 1A) were selected through reference to the contrast-based regions of interest (ROIs) marked out on the T_2-weighted MRI images (Figure 1B).

Model solutions

T_2 and diffusion coefficients were measured in fructose solutions at a pH value of 4.4 at different concentrations: 0 (pure water), 10, 20, 30, 40, 60, 80, 100 and 120 g/L (corresponding to a water content of 100, 99, 98, 97, 96, 94, 92, 90 and 89%, respectively). The 50 ml tubes (diameter 3.4 cm, height 7.0 cm) containing the solutions were placed on a specially designed base with 2mm-thick neoprene pads between the tubes and the base to prevent vibration during MRI measurements.

Magnetic Resonance Imaging

Image acquisition

MRI measurements were performed on a 1.5T scanner (Magnetom Avanto, Siemens, Erlangen, Germany) equipped with a circular polarized head array RF coil. Tomatoes were placed in a temperature-regulating device installed inside the RF coil. The temperature of the samples during the MRI measurements was 15 ± 1°C. Four optical fibers connected to a data logger (UMI8, FISO Technologies Inc., Canada) were inserted in a water-filled tube placed near the tomato slices but outside the Field of View (FoV), to monitor the temperature of the samples during the MRI experiment. MRI acquisition began when the temperature reached a steady value (about 1 h 30 min after initiating the temperature regulation). Prior to the experiment, the uncertainty of the temperature measurement was estimated to be less than 1°C.

Geometrical parameters were kept constant for all two-dimensional (2D) MRI experiments; coronal sections in the middle of the tomato slices were imaged with a slice thickness of 5 mm, a 128×128 pixel matrix and a 155×155mm² FoV. The following 2D MRI experiments were performed:

1) Transverse relaxation parameters were measured using a multi-spin echo (MSE) sequence [10] with 256 echoes, where the first echo (TE) was equal to the inter-echo spacing (TE=6.5ms). Pixel bandwidth was 260 Hz/pixel and one scan was performed. Repetition time (TR) was fixed at 20s to prevent T_1-weighting.

2) T_2* mapping was carried out with a gradient echo sequence, with 12 echoes (first echo time TE_1=2.27ms and ΔTE=1.58ms), TR=5s, BW=930Hz/pixel, flip angle=90° and 2 scans.

3) The Apparent Diffusion Coefficient (ADC) was estimated using the pulse field gradient spin echo (PFGSE) sequence with TE=91ms, TR=5s, diffusion time Δ=60ms and diffusion gradient duration δ=20ms. The b values and the respective number of scans were chosen to achieve an acceptable uncertainty on the estimated ADC in a given acquisition time. Moreover, the acquisition of a minimum of 4 points was

considered necessary to be able to verify that the data did follow a mono-exponential decay. Using an acquisition time of 1h25 min, we found that the lowest uncertainty value, estimated using the Cramer-Rao bound, was achieved for b values of 0, 97.7, 390.8 and 879.4 $s.mm^{-2}$ with, respectively, 2, 1, 1 and 4 scans. The mean uncertainty evaluated at voxel scale was $0.026x10^{-3}$ $mm^2.s^{-1}$

In addition to 2D images for parametric mapping, 3D morphological images with a spatial resolution of 0.5 x 0.5 x 0.5 mm^3 were acquired using a turbo spin echo (TSE) sequence with the following parameters: 326x384 pixel matrix, 152x180 mm^2 FoV, 64 slices, TR=144 ms, TE=29 ms, BW=200 Hz/pixel, Turbo Factor=6 and 3 scans.

T_2 and ADC measurements were performed on model solutions with the same experimental protocols as those used on tomato slices, except that the image slice was in the transverse plane and the TR was set to 10s. These acquisitions were repeated three times.

Image processing

Multi-exponential T_2 maps of the tomato slices before and after dehydration were calculated using the algorithm implemented in Matlab software described in [30], based on a discrete model with *a priori* known number of components. The method is iterative and based on the maximization of the likelihood criterion under the hypothesis of Rician noise, with spatial regularity imposed to achieve noise reduction. The number of components for the relaxation model was estimated from the relaxation time distribution spectra estimated for the equatorial pericarp and the placenta using a Maximum Entropy Method (MEM) [33] implemented in Scilab software. Only echoes characterized by SNR greater than 7 were retained for the T_2 spectra estimation, making it possible to assume a zero-mean Gaussian noise distribution in the magnitude images. T_2 spectra were computed at the scale of the regions of interest in the equatorial pericarp (three ROIs) and in the placenta (two ROIs) (Figure 1B), corresponding to the tissues taken for chemical analyses. The initial guess for the relaxation time maps was fixed at the typical values of T_2 and

their corresponding intensities I_0 to be found in the relaxation spectra of the outer pericarp of fresh tomato slices.

The intensity maps were corrected for spatial signal heterogeneities induced by the receiving coil by normalizing the I_0 maps using the image of a homogeneous reference object. The reference image was acquired with the MSE sequence under conditions identical to those used for tomatoes, with TE=6.5ms and 20 scans.

Apparent microporosity maps were estimated from T_2* and T_2 mono-exponential maps, calculated from MSE and MGE images respectively [32], on a pixel-to-pixel basis with Scilab software and using the Levenberg–Marquardt algorithm for chi-square minimization. For both T_2 and T_2*, only pixels characterized by a minimum signal to noise ratio (SNR) of 7 were retained for the estimation of the relaxation parameters. The same protocol was employed for the estimation of the mono-exponential relaxation parameters in the sugar and manganese solutions.

ADC maps were calculated on a pixel-to-pixel basis with Scilab software, using the Levenberg–Marquardt algorithm, assuming a mono-exponential model. The number of scans was considered when calculating the ADC maps by weighting each signal with a scalar proportional to the corresponding number of scans.

For numerical analyses, the mean values of T_2 and the associated relative intensities, apparent microporosity and ADC were calculated using the same ROIs (Figure 1B) as those used for the chemical analyses and the estimates of the relaxation spectra.

The dehydration-induced volume loss of the equatorial pericarp was estimated from the 3D images using the difference in pericarp volume before and after dehydration. Semi-automatic

segmentation was performed using the Avizo software [34], on every 4-5 images and then interpolated for intermediate images.

Stability of the imaging conditions

The stability of the imaging conditions between the measurements performed on fresh and dried tomatoes was estimated from the mono-exponential T_2 and I_0 measured in the manganese solution. The maximum standard deviation for T_2 and I_0 corresponded to a maximum of 0.9% and 5% of mean parameter values respectively. It was slightly higher than the standard deviation obtained from the measurements taken from the tubes of fructose solution. Indeed, the standard deviation for T_2, I_0 and ADC measurements calculated on three repetitions corresponded to a maximum of 0.5, 0.9 and 0.7% of the mean values respectively. This difference was probably due to possible slight temperature variations where measurements were performed over the course of several days.

Chemical analysis

The water content of the equatorial pericarp and placenta samples was determined by the difference in mass of the samples before and after dehydration in an oven at 70°C for 72h. After removing the samples to estimate the water content, the remainder of the pericarp and placenta tissues were placed in tubes and then centrifuged for 20 minutes at 18,672 x g (12,500 rpm) and at 4°C. The pH of the liquid phase thus obtained was then measured using a pH-meter (HI5221, Hannah Instruments, USA).

Statistical analysis of data

One-way ANOVA statistical analysis of variance was performed for the parametric MRI values (relaxation parameters (T_2 and signal intensity), diffusion coefficient and apparent microporosity) for the equatorial pericarp and placenta to determine if these parameters were statistically different ($P<0.01$) before and after dehydration. Statistical analyses were not carried out for water content or pH because the measurement protocols differed for the fresh and dried slices.

Results

Impact of sugar concentration on T_2, signal amplitude and diffusion coefficient in model solutions

The relationship between the relaxation rate R_2 ($1/T_2$), signal amplitude (I_0) and ADC and water content of fructose solutions are shown in Figure 2. The dependence of the relaxation rate (Figure 2 A) and ADC (Figure 2 B) on concentration was linear as is expected in the case of diluted solutions [25, 26]. For the range of water content analyzed (100 to 89%), T_2 decreased from 2.17 to 0.42 s (R_2 of 0.46 and 2.39 s^{-1} respectively), while ADC decreased from 1.75 to 1.37x10^{-9} $m^2.s^{-1}$. By contrast, the signal amplitude (I_0) (Figure 2 A) was not sensitive to variations in water content in the water content range studied.

Water content and pH

The water content and pH values measured in the equatorial pericarp and the placenta of tomatoes before and after drying are shown in Table 2. In the case of fresh tissues, water content was similar for the equatorial pericarp and the placenta (from about 93 to 95 %). Dehydration in a cold room (regime 1) appeared to induce higher water content decrease in the pericarp than in the placenta (about 4 and 2% respectively), while water content decrease was similar (about 3%) for these two tissues for regime 2. In the case of dehydration in a vacuum oven (regime 3), the decrease in water content in both pericarp and placenta tissues was relatively low (from 2 to 1%) compared to regimes 1A and 2 (from 4 to 3%).

pH values (Table 2) were similar in the equatorial pericarp before and after dehydration using the cold room and ventilated oven regimes, while dehydration using a vacuum oven induced a slight decrease in pH.

Morphological characteristics

A decrease in the surface area of the tomato slices can be observed from the 3D images (Figure 3) for the four dehydration modalities studied, by comparing coronal and transverse sections of the tomato slices before and after dehydration. In the case of regimes 1 and 2, dehydration appears to affect all tomato tissues similarly. By contrast, under regime 3, the dehydration process led to the disappearance of the locular tissue while other tissues appeared less impacted. This is consistent with the lower level of water loss in the pericarp and the placenta observed for regime 3 (Table 2), compared to other dehydration regimes.

Volumes of the equatorial pericarp of the tomato slices before and after dehydration are shown in Table 3. For regimes 1A and 2, a similar decrease in volume was recorded (49 and 48% respectively), while it was smaller under regime 1B (39%) as expected given the lower mass loss recorded for this regime. Dehydration in a vacuum oven (regime 3) generated the smallest pericarp volume loss (26%) in line with the particular impact of the drying process on the locular tissue (Figure 3).

Spatial distribution of relaxation parameters, diffusion coefficient and apparent microporosity

The preliminary analyses by MEM algorithm showed that the transverse relaxation signal followed a tri-exponential pattern for both types of tissue before and after dehydration, indicating that three water pools could be distinguished. The tri-exponential model was therefore used for T_2 mapping. Typical examples of the tri-exponential transverse relaxation maps for the tomato slices before and after dehydration using regime 1-A are shown in Figures 4 A and B. Reference tubes are not shown on these

images because the multi-exponential relaxation model is not suitable for manganese solutions leading to outliers. For fresh tissues, T_{21} was around 40 ms throughout the slice and consequently did not permit differentiation of the tissues. By contrast, the T_{22} maps allowed the placenta (T_{22}≈180 ms) to be distinguished from the pericarp (T_{22}≈400 ms) and the locular (T_{22}≈480 ms) tissues. The T_{23} maps also allowed the placenta (T_{23}≈450 ms), the pericarp (T_{23}≈700 ms) and the locular tissues (T_{23}≈ 800 ms) to be distinguished. Moreover, a ring-shaped tissue with a shorter T_{23} can be observed in the pericarp, which probably corresponds to vascular bundles. On the I_{01} maps of fresh tomato slices (Figure 4 B) it was barely possible to differentiate the tissues, while in the I_{02} and I_{03} maps it was possible to distinguish the placenta from the other tissues. Indeed, I_{02} had a higher value in the placenta than in the pericarp and locular tissues, while the opposite was observed for I_{03}.

Dehydration did not impact the T_{21} and I_{01} maps to any marked degree, but induced significant changes in the second and third relaxation component maps. Indeed, both T_{22} and T_{23} decreased noticeably in the equatorial pericarp and the locular tissues, while they remained unchanged in the placenta. Unexpectedly, dehydration induced a marked increase in I_{02}, and appears to reduce I_{02} differences within the tissues. Last, I_{03} decreased for all tissues as a consequence of dehydration.

Mean values of multi-exponential relaxation parameters calculated using the ROIs in the equatorial pericarp and in the placenta (Figure 1) are shown for the different dehydration regimes in Tables 4 A and B respectively. The total intensity of the relaxation signal (I_{TOT}, defined as the sum of I_{01}, I_{02} and I_{03}) of the pericarp was not affected by dehydration, as expected on the basis of the experiment on the model solutions (Figure 2 A). By contrast, the intensity of the relaxation components differed between fresh and dried tissues. I_{01} significantly increased for most of the regimes studied, with the exception of regime 1-A, where it remained stable. I_{02} increased strongly after dehydration, with the degree varying according to drying regime (69, 51, 69 and 27% for dehydration regimes 1-A, 1-B, 2 and 3 respectively). I_{03} decreased

by about 20-25% regardless of drying regime. This accords with observations from the relaxation maps shown for regime 1-A (Figure 5). Relaxation time, T_{21} was not affected by water loss, whatever the dehydration regime, remaining stable at around 30-40ms. The T_{22} of tissues dried using regimes 1-A, 2 and 3 decreased by approximately 30-35% while the T_{22} of tissues dried using regime 1-B remained stable. The T_{23} of tissues dried using regime 1-A and 2 decreased in similar proportions (28%), while a smaller decrease in T_{23} after dehydration using regime 1-B was observed (9%). Conversely, the T_{23} of tissues dried in a vacuum oven (regime 3) increased slightly (7%). Thus, for the pericarp, similar variations of T_{22}, T_{23}, I_{02} and I_{03} were observed for regimes 1-A and 2. This agreed with a similar decrease in the water content of the pericarp tissue (4.1 and 3.3% respectively (Table 2)) and with the corresponding observed volume losses (49 and 48% (Table 3)). The variations in T_2 and I_0 differed slightly for regime 1-B (a volume loss of 39% and water content decrease of 2.2%) and were very different for regime 3 (with a volume loss of 26% and a decrease in water content of 1.8%). The variations in relative intensities observed for all regimes demonstrate a potential link to changes in the distribution of water within the tissues caused by dehydration.

I_{TOT} in the placenta increased following dehydration for all regimes except for drying in a vacuum oven (regime 3). I_{01} did not vary, except for regime 2 where it increased by approximately 50%. I_{02} increased with dehydration regardless of drying conditions. This increase varied between 35%, 28%, 50% and 53% respectively for regimes 1-A, 1-B, 2 and 3. Last, I_{03} decreased slightly with dehydration for regimes 1-A and 2 (8%), while it remained stable for the other two drying regimes. For the pericarp, T_{21} values were around 30-40ms and remained stable regardless of dehydration regime. Meanwhile, the T_{22} of tissues dried using regimes 1-A and 2 remained stable with drying, whereas for regimes 1-B and 3, T_{22} increased after dehydration (37% and 55% respectively). Last, the T_{23} of tissues dried using regimes 1-A and 2 remained stable or decreased slightly (9%), whereas T_{23} increased in tissues dried using regimes 1-B and 3 (16% and 39% respectively).

The ADC map for fresh tissues (Figure 5A) allowed the placenta to be distinguished from the other tomato tissues. However, a preliminary analysis showed that the experimental points considerably deviated from the expected linear relationship between *ln(I(b)/I(b=0))* and *b* . This deviation was explained by the relatively high porosity of the placenta, which could be expected to introduce an additional spin dephasing effect because of the susceptibility induced magnetic field gradients created at the air/water interfaces. The ADC of the placenta was therefore excluded from the analyses. Dehydration did not induce noticeable variations in the ADC of the pericarp and the locular tissues. This was confirmed by numerical analyses of the mean values calculated using the ROIs (Figure 1). In fresh tomato pericarp, the ADC was about (1.42-1.43 $x10^{-9}$ m^2s^{-1}) and did not change significantly ($P < 0.01$) for any dehydration regime.

An example of the apparent microporosity map of fresh tomato is shown in Figure 5 B. The highest microporosity level was measured in the placenta (9-11%), while it was about 2-3% in the equatorial and radial pericarps and appeared null in the locular tissue. These results are comparable to those obtained in a previous study [32]. Following dehydration, the apparent microporosity maps contained magnetic susceptibility artefacts and could therefore not be used.

Discussion

The method described in [30] allowed multi-T_2 relaxation parameter maps to be estimated, making it possible to access information on different water pools in each voxel. This approach has made possible interesting observations that could not be carried out using mono-exponential relaxation maps. First, independently of drying regime, the optimal relaxation signal model for dehydrated tomatoes was observed to be tri-exponential, as for fresh fruit, showing that the cell membranes were still acting as semi-permeable barriers and that water exchanges between compartments were slow or intermediate compared to T_2. An unexpected result was obtained concerning the variations in the intensity of the multi-

exponential signal components (Table 4). While I_{TOT} was stable or only slightly affected by dehydration in the case of the pericarp and placenta tissue respectively, I_{03} markedly decreased in favor of I_{02}. Meanwhile, both T_{23} and T_{23} decreased. This indicates us that the variations in the relaxation signal cannot be explained using a relaxation model that relates each signal component to a specific cell water compartment [2-4]. One hypothesis that might explain these results is that the second and third peaks correspond to the vacuoles of two cell populations with distinct volume distributions, as has been recently proposed for tomato [18] and peach fruit [14] and oilseed rape leaves [7] and supported by tissue observations [31]. According to this hypothesis, variations in relaxation times correspond to the higher impact of the dehydration process on larger cells. Thus, we can postulate that dehydration induced a decrease in the number of large cells relative to that of small cells, consistent with the variations in I_{03} and I_{02}. The validation of this hypothesis would require additional analyses, including observations of tissue by microscopy or macro vision and/or restricted diffusion measurements of specific water fractions. In both cases, the aim would be to provide information about the size of the compartment. It would also help in elucidating the attribution of the first relaxation component to a particular water pool, which could be either non-vacuolar water (wall/extracellular water, cytoplasm, …) or water in small vascular bundles. In this attribution, the increase of I_{03} following dehydration should be taken into account.

A comparison of the results of the present experiment with the NMR experiment 100MHz [3] on carrot drying revealed some similarities. Indeed, in [3] the relative intensity of the longest relaxation time (T_{23}) component decreased when that associated with T_{22} increased, in agreement with observations in the present experiment. T_{23} decreased monotonically with drying time while T_{22} increased during the first 60 minutes and then decreased. These results were explained by both a shrinkage in the vacuolar compartment caused by water loss and the progressive concentration of sugars in the remaining vacuolar fluid. The interpretation proposed in the present study taking cell size distribution into account also appears to be of value.

According to the results obtained from the fructose solutions (Figure 2 A), the total intensity of the relaxation signal in tomato tissues could be expected to remain unchanged for the slight decrease in water content measured in tomatoes tissues. This was the case for the pericarp tissue, while I_{TOT} increased by about 10 % in placenta that had been dehydrated in the cold room and the ventilated oven. This could be explained by a possible decrease in the microporosity of the tissue, which was initially relatively high (~9-11%) compared to that of the pericarp (~2%). The decrease in placenta microporosity could also explain why T_{22} and T_{23} remained constant or decreased only slightly following drying. Indeed, it has been observed that microporosity leads to a reduction in T_2 relaxation times via the effects of magnetic susceptibility [35].

Relating variations in transverse relaxation parameters to an isolated factor is far from straightforward due to the concomitant changes in the composition and structure of tissues that occur during the dehydration process. Changes in the composition of the liquids enclosed in cell compartments affect the bulk transverse relaxation via chemical exchange effects. The results obtained from the model solutions at the same pH as that measured in tomatoes, provide an approximation of the expected variations in T_2. This approximation is only possible for dehydration regimes 1 and 2 where pH was not impacted, because a small variation in pH will give rise to considerable variations in T_2 [25, 36]. Figure 6 shows the relaxation rates of the most intense peak ($1/T_{23}$) associated with large vacuoles plotted against tissue water content for the equatorial pericarp (Figure 6 A) and the placenta (Figure 6 B). It was assumed that drying mainly affected this water pool. In the case of the pericarp, relaxation rate ($1/T_{23}$) appears to follow a linear trend with the tissue water content. By contrast, $1/T_{23}$ appeared not to vary with water content in the case of the placenta. This result can be explained by the porous structure of this tissue (Figure 5 B), see above. It is important to note that the water content of the vacuoles of large cells can be approximated only roughly by that of the tissue because, in fleshy fruit parenchyma, approximately 50% of the dry matter corresponds to a soluble compound mainly contained in the vacuole water pool [16, 37],

but also because not all of the water is located in the vacuoles of large cells. Hence, it is not possible to deduce the vacuolar water content directly from the tissue water content, especially given that the proportion of water contained in this compartment appears to be affected by drying.

Figure 7 shows the relaxation rates associated with the vacuoles of large cells (T_{23}) plotted against the inverse of the cube root of the pericarp volume, assuming a relationship between the radius of large cell vacuoles and pericarp volume. A slight increase in $1/T_{23}$ with the inverse of cell size is observed for regimes 1 and 2, corresponding to an increase in T_2 of approximately 200 ms for an increase in cell size of the order of 25%. Figure 7 demonstrates that compartment size contributes to T_2 relaxation via the loss of water magnetization at the compartment membrane. However, as stated above, it is important to note that the reasoning applied can only be an approximation as the pericarp did not consist only of large cells and because their relative size appears to be affected by drying. In order to elucidate this further, the results of the present study were compared to the relaxation time measurements in apple and peach fruit [14] under very similar experimental conditions (using the same B_0 and TE), by setting the diameter of the cell tomato parenchyma at 280µm, in line with the value reported in [31]. Here, the T_{23} values measured in fresh and dried tomato pericarps (regime 1-A, 727 and 526 ms respectively), are consistent with the variations expected from the relationship between 3/R and $1/T_2$, with R-radius, from [14]. This shows that, although the variation in cell size is not the only mechanism that could explain the T_2 variations, cell size seems to have a dominant impact on T_2 values for tissues with little porosity.

Conclusion

This experiment is the first to have used multi-exponential T_2 maps to study fruit that has undergone dehydration. Combined with microporosity maps and morphological images, these have constituted an original approach to the spatial analysis of a microstructure and macroscopic changes of

heterogeneous fruit tissues. The application of different dehydration regimes to tomatoes and analysis of two types of tissue has made it possible to draw a number of conclusions.

Total signal intensity, corresponding to the proton density of the water molecules, was not sensitive to variations in water content in the case of slight and moderate dehydration and therefore cannot be used as an indicator of water loss. On the other hand, the analysis of multi-exponential relaxation times provided information on water loss from particular water fractions. By considering variation in both relaxation times and associated signal intensities, we suggested that the multi-exponential relaxation signal reflects cell compartmentation and heterogeneity of tomato tissues at the voxel level. The later sustains the hypothesis that for the interpretation of relaxation times, cell size distribution should be considered, even at voxel scale. Under the assumption proposed for interpreting relaxation data, the MRI results appear to show that the dehydration process mainly affected large cells. Further experiments, providing information about cell size, would be necessary to validate this hypothesis.

The decrease in T_{22} and T_{23} of the equatorial pericarp were probably the result of two relaxation mechanisms occurring in parallel, namely chemical exchanges resulting from variations in solute concentration and surface relaxation resulting from a decrease in the surface to volume ratio of the compartments. As these phenomena are inherently linked in the drying process, they cannot be distinguished from each other. An alternative way to access information on water content in specific cell compartments would be to measure the diffusion coefficient over short diffusion distances. Indeed, the fact that the ADC in dilute regimes is sensitive to solute concentration alone can be directly related to water content. For these cases, 2D D-T_2 relaxometry experiments should be performed, making it possible to access the diffusion coefficients of specific water pools.

Acknowledgements

Part of this work has been performed using the PRISM core facility (Biogenouest, Univ Rennes, Univ Angers, INRAE, CNRS, FRANCE).

Declarations

Funding

This work was funded in part by the Région Bretagne.

Conflicts of interest

The authors have no conflicts of interest to declare.

References

[1] B. Hills, G. Le Floc'h, NMR studies of non-freezing water in cellular plant tissue, Food Chemistry, 51 (1994) 331-336.

[2] B.P. Hills, B. Remigereau, NMR studies of changes in subcellular water compartmentation in parenchyma apple tissue during drying and freezing, International journal of food science & technology, 32 (1997) 51-61.

[3] B. Hills, K. Nott, NMR studies of water compartmentation in carrot parenchyma tissue during drying and freezing, Applied Magnetic Resonance, 17 (1999) 521-535.

[4] J. Snaar, H. Van As, Probing water compartments and membrane permeability in plant cells by 1H NMR relaxation measurements, Biophysical Journal, 63 (1992) 1654-1658.

[5] M.E. Gonzalez, D.M. Barrett, M.J. McCarthy, F.J. Vergeldt, E. Gerkema, A.M. Matser, H. Van As, 1H-NMR study of the impact of high pressure and thermal processing on cell membrane integrity of onions, Journal of food science, 75 (2010) E417-E425.

[6] M. Musse, L. De Franceschi, M. Cambert, C. Sorin, F. Le Caherec, A. Burel, A. Bouchereau, F. Mariette, L. Leport, Structural changes in senescing oilseed rape leaves at tissue and subcellular levels monitored by nuclear magnetic resonance relaxometry through water status, Plant physiology, 163 (2013) 392-406.

[7] C. Sorin, M. Musse, F. Mariette, A. Bouchereau, L. Leport, Assessment of nutrient remobilization through structural changes of palisade and spongy parenchyma in oilseed rape leaves during senescence, Planta, 241 (2015) 333-346.

[8] C. Sorin, F. Mariette, M. Musse, L. Leport, F. Cruz, J.-C. Yvin, Leaf Development Monitoring and Early Detection of Water Deficiency by Low Field Nuclear Magnetic Resonance Relaxation in Nicotiana tabacum Plants, Applied Sciences, 8 (2018) 943.

[9] C. Sorin, F. Mariette, M. Musse, NMR study of fresh cut salads: influence of temperature and storage time on leaf structure and water distribution in escarole, Magnetic Resonance in Chemistry, (2019).

[10] H. Adriaensen, M. Musse, S. Quellec, A. Vignaud, M. Cambert, F. Mariette, MSE-MRI sequence optimisation for measurement of bi-and tri-exponential T2 relaxation in a phantom and fruit, Magnetic resonance imaging, 31 (2013) 1677-1689.

[11] H. Van As, J. van Duynhoven, MRI of plants and foods, J Magn Reson, 229 (2013) 25-34.

[12] G. Winisdorffer, M. Musse, S. Quellec, M.-F. Devaux, M. Lahaye, F. Mariette, MRI investigation of subcellular water compartmentalization and gas distribution in apples, Magnetic Resonance Imaging, 33 (2015) 671-680.

[13] F. Xu, X. Jin, L. Zhang, X.D. Chen, Investigation on water status and distribution in broccoli and the effects of drying on water status using NMR and MRI methods, Food Research International, 96 (2017) 191-197.

[14] M. Musse, K. Bidault, S. Quellec, B. Brunel, G. Collewet, M. Cambert, N. Bertin, Spatial and temporal evolution of quantitative magnetic resonance imaging parameters of peach and apple fruit–relationship with biophysical and metabolic traits, The Plant Journal, 105 (2021) 62-78.

[15] H. Van As, Intact plant MRI for the study of cell water relations, membrane permeability, cell-to-cell and long distance water transport, Journal of Experimental Botany, 58 (2006) 743-756.

[16] M. Musse, S. Quellec, M. Cambert, M.-F. Devaux, M. Lahaye, F. Mariette, Monitoring the postharvest ripening of tomato fruit using quantitative MRI and NMR relaxometry, Postharvest Biology and Technology, 53 (2009) 22-35.

[17] H. Van As, T. Scheenen, F.J. Vergeldt, MRI of intact plants, Photosynthesis Research, 102 (2009) 213.

[18] R. Leforestier, F. Mariette, M. Musse, MRI Study of Temperature Dependence of Multi-exponential Transverse Relaxation Times in Tomato, Applied Magnetic Resonance, (2021) 1-18.

[19] V. Panarese, L. Laghi, A. Pisi, U. Tylewicz, M. Dalla Rosa, P. Rocculi, Effect of osmotic dehydration on Actinidia deliciosa kiwifruit: A combined NMR and ultrastructural study, Food chemistry, 132 (2012) 1706-1712.

[20] N. Proietti, G. Adiletta, P. Russo, R. Buonocore, L. Mannina, A. Crescitelli, D. Capitani, Evolution of physicochemical properties of pear during drying by conventional techniques, portable-NMR, and modelling, Journal of food engineering, 230 (2018) 82-98.

[21] Y. Chen, H. Dong, J. Li, L. Guo, X. Wang, Evaluation of a nondestructive NMR and MRI method for monitoring the drying process of gastrodia elata blume, Molecules, 24 (2019) 236.

[22] S. Cheng, R. Li, H. Yang, S. Wang, M. Tan, Water status and distribution in shiitake mushroom and the effects of drying on water dynamics assessed by LF-NMR and MRI, Drying Technology, 38 (2020) 1001-1010.

[23] L. Cui, Y. Chen, M. Li, T. Liu, P. Yang, L. Guo, X. Wang, Detection of water variation in rosebuds during hot-air drying by LF-NMR and MRI, Drying Technology, (2019).

[24] B. Hills, S. Duce, The influence of chemical and diffusive exchange on water proton transverse relaxation in plant tissues, Magnetic resonance imaging, 8 (1990) 321-331.

[25] R. Leforestier, F. Mariette, M. Musse, Impact of chemical exchange on transverse relaxation at low and moderate magnetic field strengths for sugar solutions representative of fruit tissues analyzed by simulation and MRI experiments, Journal of Magnetic Resonance, 322 (2021) 106872.

[26] N.N. Yadav, J. Xu, A. Bar-Shir, Q. Qin, K.W. Chan, K. Grgac, W. Li, M.T. McMahon, P.C. van Zijl, Natural D-glucose as a biodegradable MRI relaxation agent, Magnetic resonance in medicine, 72 (2014) 823-828.

[27] E. Simon, Phospholipids and plant membrane permeability, New Phytologist, 73 (1974) 377-420.

[28] G. Lester, E. Stein, Plasma membrane physicochemical changes during maturation and postharvest storage of muskmelon fruit, Journal of the American Society for Horticultural Science, 118 (1993) 223-227.

[29] I.N. Ramos, T.R.S. Brandão, C.L.M. Silva, Structural Changes During Air Drying of Fruits and Vegetables, Food Science and Technology International, 9 (2003) 201-206.

[30] C. El-Hajj, S. Moussaoui, G. Collewet, M. Musse, Multi-exponential Transverse Relaxation Times Estimation from Magnetic Resonance Images under Rician Noise and Spatial Regularization, IEEE Transactions on Image Processing, (2020).

[31] D. Legland, M.F. Devaux, B. Bouchet, F. Guillon, M. Lahaye, Cartography of cell morphology in tomato pericarp at the fruit scale, Journal of Microscopy, 247 (2012) 78-93.

[32] M. Musse, F. De Guio, S. Quellec, M. Cambert, S. Challois, A. Davenel, Quantification of microporosity in fruit by MRI at various magnetic fields: comparison with X-ray microtomography, Magnetic resonance imaging, 28 (2010) 1525-1534.

[33] F. Mariette, J. Guillement, C. Tellier, P. Marchal, Continuous relaxation time distribution decomposition by MEM, in: Data handling in science and technology, Elsevier, 1996, pp. 218-234.

[34] T.F. Scientific, Avizo Software for Materials Science, https://www.thermofisher.com/fr/fr/home/industrial/electron-microscopy/electron-microscopy-instruments-workflow-solutions/3d-visualization-analysis-software/avizo-materials-science.html.

[35] H. Donker, H. Van As, H. Edzes, A. Jans, NMR imaging of white button mushroom (Agaricus bisporis) at various magnetic fields, Magnetic Resonance Imaging, 14 (1996) 1205-1215.

[36] B.P. Hills, Nuclear magnetic resonance relaxation studies of proton exchange in methanol–water mixtures, Journal of the Chemical Society, Faraday Transactions, 86 (1990) 481-487.

[37] C. Agius, S. von Tucher, B. Poppenberger, W. Rozhon, Quantification of sugars and organic acids in tomato fruits, MethodsX, 5 (2018) 537-550.

Tables

REGIME	METHOD	DURATION	TEMPERATURE (°C)	WEIGHT LOSS (%)
1-A	COLD ROOM	7 DAYS	4	38±1
1-B	COLD ROOM	5 DAYS	4	30±1

2	VENTILATED OVEN	9 HOURS	35	40±1
3	VACUUM OVEN	23 HOURS	35	44±2

Table 1: Average mass loss for tomato slices depending on drying regime (method, duration, temperature)

DRYING REGIME	WATER CONTENT (%)				pH EQUATORIAL PERICARP	
	EQUATORIAL PERICARP		PLACENTA			
	FRESH	DEHYDRATED	FRESH	DEHYDRATED	FRESH	DEHYDRATED
1-A	94.7±0.2	90.6±0.1	94.0± 0.4	91.8± 0.1	4,2 ± 0,1	4,2 ± 0,0
1-B	94.1±0.1	91.9±0.5	93.4± 0.1	92.0± 0.2	4,4 ± 0,1	4,4 ± 0,1
2	95.4±0.1	92.1±0.5	94.5±0.1	90.9± 0.6	4,5 ± 0,1	4,5 ± 0,1
3	95.0±0.2	93.2±0.5	94.2± 0.0	93.7±0.5	4,4 ± 0,0	4,0 ± 0,1

Table 2: Water content and pH of tomato samples, before and after dehydration. In the case of fresh tomatoes, the means and standard deviations were calculated from four values, each corresponding to a different tomato. In the case of dried tissues, the means and standard deviations were calculated from 12 values for the pericarp (3 per tomato) and 8 values for the placenta (2 per tomato).

DRYING REGIME	VOLUME x 10^{-5} (m^3)		DIFFERENCE (%)
	FRESH	DEHYDRATED	
1-A	2.32±0.08	1.18±0.03	49
1-B	2.52±0.26	1.54±0.18	39
2	2.37±0.20	1.24±0.08	48
3	2.53±0.09	1.88±0.04	26

Table 3: Equatorial pericarp volumes before and after dehydration computed from 3D TSE MRI images. Means and standard deviations are calculated from four values, each corresponding to a different tomato.

A

REGIME 1-A											
	I_{TOT} (u.a.)	**I_{01} (u.a.)**	**I_{01} (%)**	**T_{21} (ms)**	**I_{02} (u.a.)**	**I_{02} (%)**	**T_{22} (ms)**	**I_{03} (u.a.)**	**I_{03} (%)**	**T_{23} (ms)**	**ADC ($10^{-9}m^2.s^{-1}$)**
FRESH	1629±80	100±42	6±2	40±14	373±20	23±1	414±39	1156±59	71±2	727±69	1.43±0.05
DRIED	1655±143	150±47	9±2	33±7	628±41	38±1	293±26	877±70	53±1	526±42	1.38±0.05

P	0.579	0.011	0.004	0.165	0.000	0.000	0.000	0.000	0.000	0.000	0.032
DIFFERENCE	N.S.	N.S.	48%	N.S.	69%	66%	-29%	-24%	-25%	-28%	N.S.
REGIME 1-B											
	I_{TOT} (u.a.)	**I_{01} (u.a.)**	**I_{01} (%)**	**T_{21} (ms)**	**I_{02} (u.a.)**	**I_{02} (%)**	**T_{22} (ms)**	**I_{03} (u.a.)**	**I_{03} (%)**	**T_{23} (ms)**	**ADC ($10^{-9}m^2.s^{-1}$)**
FRESH	1605±98	75±46	5±2	31±8	405±22	25±1	390±18	1125±52	70±2	690±46	1.42±0.05
DRIED	1676±116	141±60	8±3	29±8	611±33	37±2	370±34	923±49	55±2	628±50	1.41±0.04
P	0.132	0.007	0.003	0.421	0.000	0.000	0.082	0.000	0.000	0.005	0.713
DIFFERENCE	N.S.	87%	81%	N.S.	51%	45%	N.S.	-18%	-21%	-9%	N.S.

REGIME 2											
	I_{TOT} (u.a.)	**I_{01} (u.a.)**	**I_{01} (%)**	**T_{21} (ms)**	**I_{02} (u.a.)**	**I_{02} (%)**	**T_{22} (ms)**	**I_{03} (u.a.)**	**I_{03} (%)**	**T_{23} (ms)**	**ADC ($10^{-9}m^2.s^{-1}$)**
FRESH	1597±100	74±54	4±3	27±7	360±21	23±1	465±27	1164±55	73±2	772±45	1.42±0.08
DRIED	1698±196	154±64	9±3	32±9	607±84	36±2	314±19	938±86	55±2	554±30	1.41±0.06
P	0.126	0.003	0.001	0.176	0.000	0.000	0.000	0.000	0.000	0.000	0.664
DIFFERENCE	N.S.	109%	99%	N.S.	69%	58%	-32%	-19%	-24%	-28%	N.S.

REGIME 3											
	I_{TOT} (u.a.)	**I_{01} (u.a.)**	**I_{01} (%)**	**T_{21} (ms)**	**I_{02} (u.a.)**	**I_{02} (%)**	**T_{22} (ms)**	**I_{03} (u.a.)**	**I_{03} (%)**	**T_{23} (ms)**	**ADC ($10^{-9}m^2.s^{-1}$)**
FRESH	1627±80	99±49	6±3	43±18	386±16	24±1	403±34	1142±56	70±2	696±44	1.43±0.04
DRIED	1693±139	230±39	14±1	40±6	491±29	29±1	260±28	972±85	57±1	745±33	1.47±0.04
P	0.171	0.000	0.000	0.670	0.000	0.000	0.000	0.000	0.000	0.006	0.036
DIFFERENCE	N.S.	132%	125%	N.S.	27%	22%	-36%	-15%	-18%	7%	N.S.

B

REGIME 1-A										
	I_{TOT} (u.a.)	**I_{01} (u.a.)**	**I_{01} (%)**	**T_{21} (ms)**	**I_{02} (u.a.)**	**I_{02} (%)**	**T_{22} (ms)**	**I_{03} (u.a.)**	**I_{03} (%)**	**T_{23} (ms)**
FRESH	1421±32	128±21	9±1	34±5	463±25	33±2	176±32	830±37	58±2	449±79
DRIED	1537±48	144±19	9±1	35±8	626±14	41±1	196±26	768±34	50±1	431±47

P	0,000	0,127	0,555	0,764	0,000	0,000	0,197	0,003	0,000	0,590
DIFFERENCE	8%	N.S.	N.S.	N.S.	35%	25%	N.S.	-8%	-15%	N.S.
REGIME 1-B										
	I_{TOT} (u.a.)	**I_{01} (u.a.)**	**I_{01} (%)**	**T_{21} (ms)**	**I_{02} (u.a.)**	**I_{02} (%)**	**T_{22} (ms)**	**I_{03} (u.a.)**	**I_{03} (%)**	**T_{23} (ms)**
FRESH	1382±29	103±26	7±2	35±8	460±23	33±2	164±27	819±43	59±3	438±42
DRIED	1508±21	145±31	10±2	36±9	589±13	39±1	225±35	775±32	51±2	509±52
P	0,000	0,011	0,039	0,906	0,000	0,000	0,002	0,034	0,000	0,010
DIFFERENCE	9%	N.S.	N.S.	N.S.	28%	17%	37%	N.S.	-13%	16%

REGIME 2										
	I_{TOT} (u.a.)	**I_{01} (u.a.)**	**I_{01} (%)**	**T_{21} (ms)**	**I_{02} (u.a.)**	**I_{02} (%)**	**T_{22} (ms)**	**I_{03} (u.a.)**	**I_{03} (%)**	**T_{23} (ms)**
FRESH	1424±12	86±24	6±2	34±7	420±18	29±1	219±19	919±22	65±2	449±20
DRIED	1610±55	133±34	8±2	29±7	630±11	39±2	214±16	847±37	53±1	408±30
P	0,000	0,006	0,025	0,168	0,000	0,000	0,590	0,000	0,000	0,006
DIFFERENCE	13%	56%	N.S.	N.S.	50%	33%	N.S.	-8%	-18%	-9%

REGIME 3										
	I_{TOT} (u.a.)	**I_{01} (u.a.)**	**I_{01} (%)**	**T_{21} (ms)**	**I_{02} (u.a.)**	**I_{02} (%)**	**T_{22} (ms)**	**I_{03} (u.a.)**	**I_{03} (%)**	**T_{23} (ms)**
FRESH	1428±38	123±13	9±1	37±9	447±22	31±1	164±19	859±29	60±1	409±39
DRIED	1524±124	127±13	8±1	49±16	682±36	45±5	254±39	715±145	47±6	569±26
P	0,058	0,543	0,621	0,085	0,000	0,000	0,000	0,016	0,000	0,000
DIFFERENCE	N.S.	N.S.	N.S.	N.S.	53%	44%	55%	N.S.	-23%	39%

Table 4, A and B: Means and standard deviations of the transverse relaxation parameters of the equatorial pericarp (A) and placenta (B), before and after dehydration for all regimes. Shaded fields indicate cases for which the difference (%) between parameters measured in fresh and dried tissue is significant (P <0.01). F-test value (Difference) and probability for the null hypothesis (P) are shown for each MRI parameter.

Figures

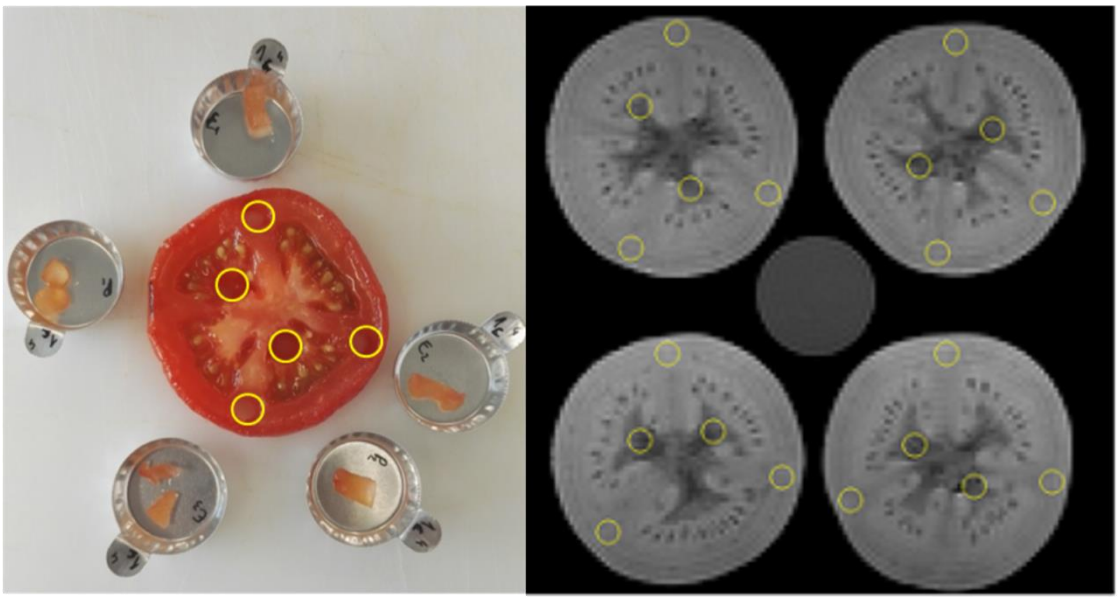

Figure 1, A: Picture showing the samples extracted for destructive analyses, selected to correspond to the ROIs used in the computation of MRI parameters. B: MRI image of dehydrated tomato slices (MSE, TE = 78ms, modality 1-A) with regions of interest (ROIs) in the equatorial pericarp (3 ROIs) and placenta (2 ROIs).

A

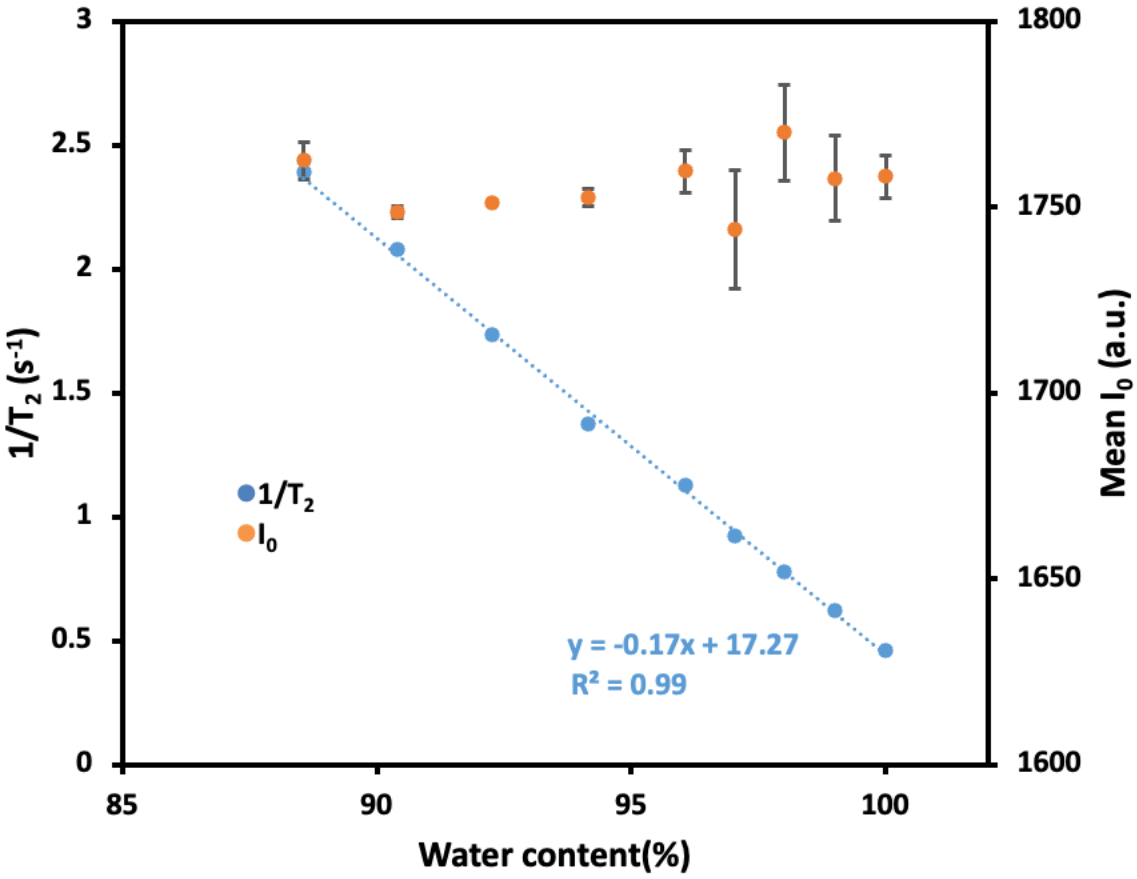
3
2.5
2
1.5
1
0.5
0
1800
1750
1700
1650
1600
85
90
95
100
1/T2 (s-1)
Mean I0 (a.u.)
Water content(%)
1/T2
I0
y = -0.17x + 17.27
R² = 0.99

B

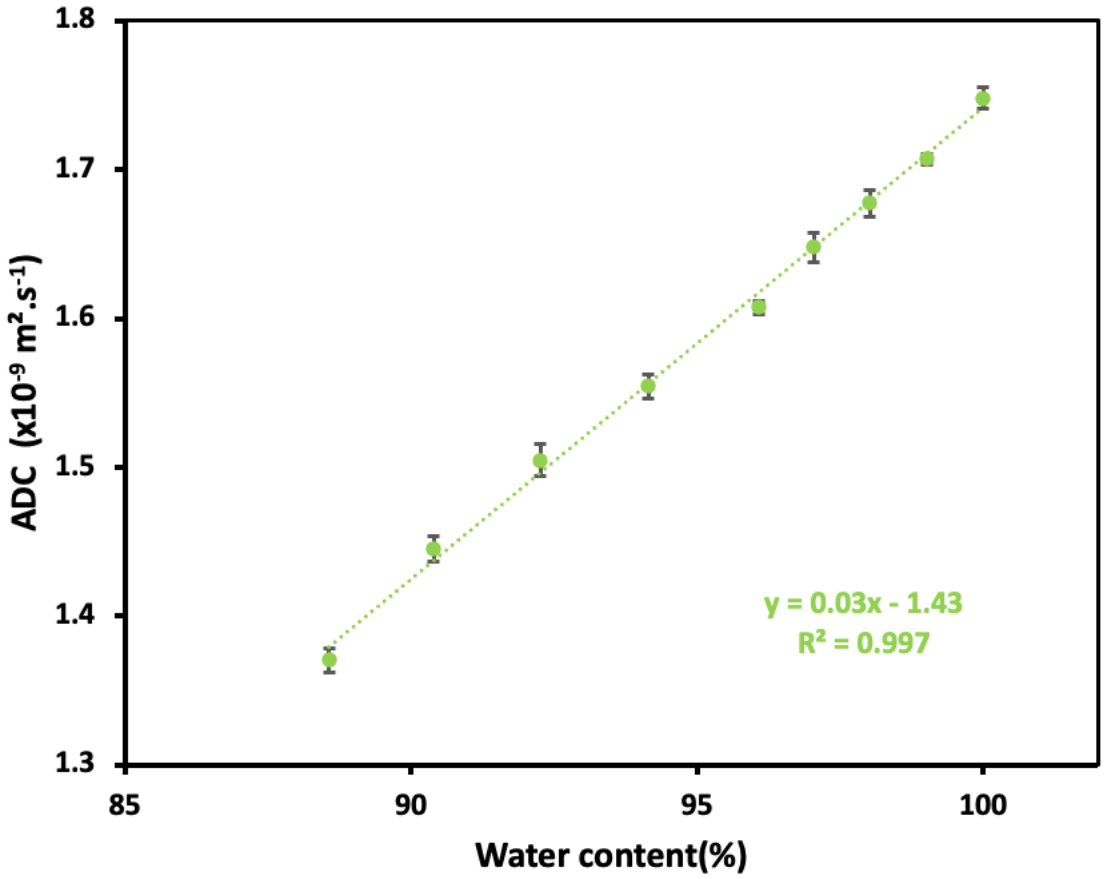

Figure 2, A: Relaxation rates $1/T_2$ (●) and mean signal intensities I_0 (●) of an aqueous solution of fructose at pH 4.4 and at 16°C±1°C as a function of water content. B: ADC (●) of an aqueous solution of fructose at pH 4.4 and at 16°C±1°C as a function of water content. The data were obtained from mono-exponentials I_0 and T_2 maps, and correspond to the mean values of 3 repetitions measured on the plotted ROIs in tubes.

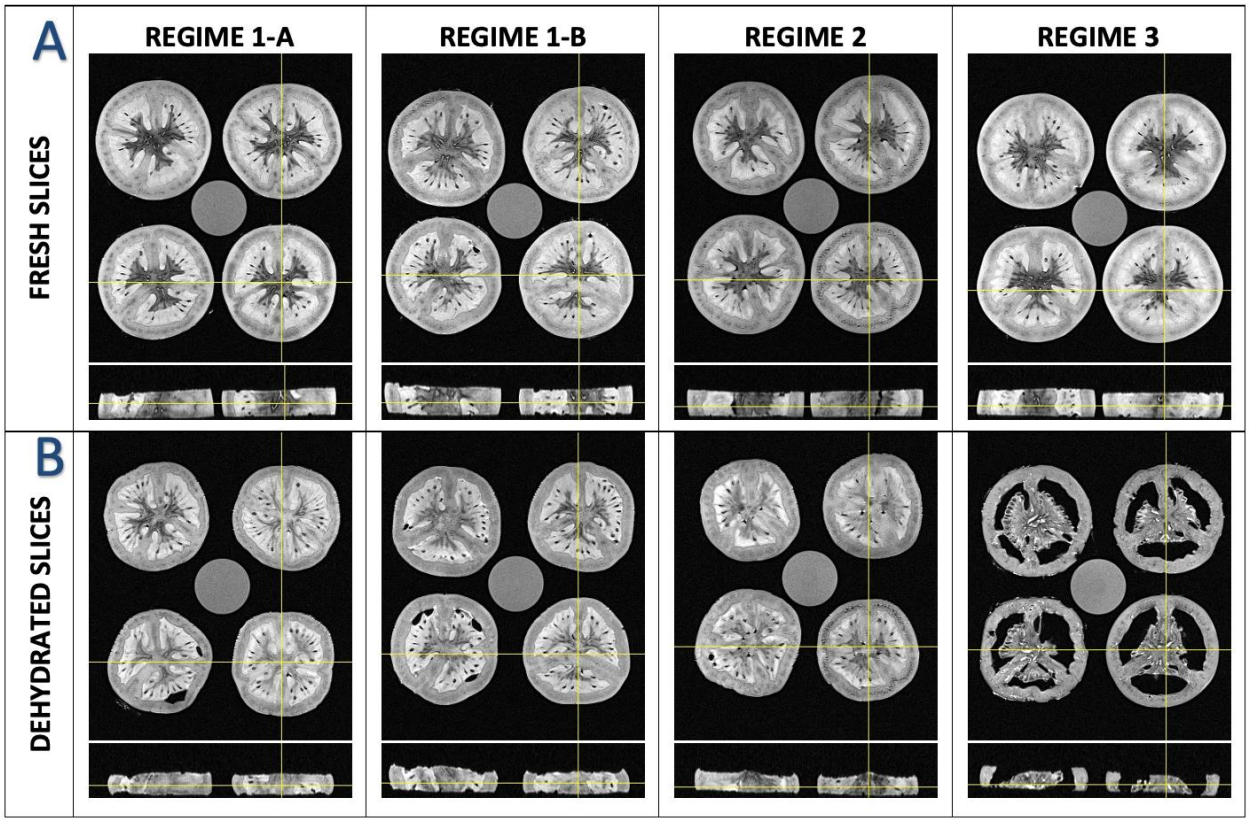

Figure 3: Coronal (top) and transverse (bottom) sections of TSE-3D MRI images from fresh (A) and dehydrated (B) tomato slices for each dehydration regime

A

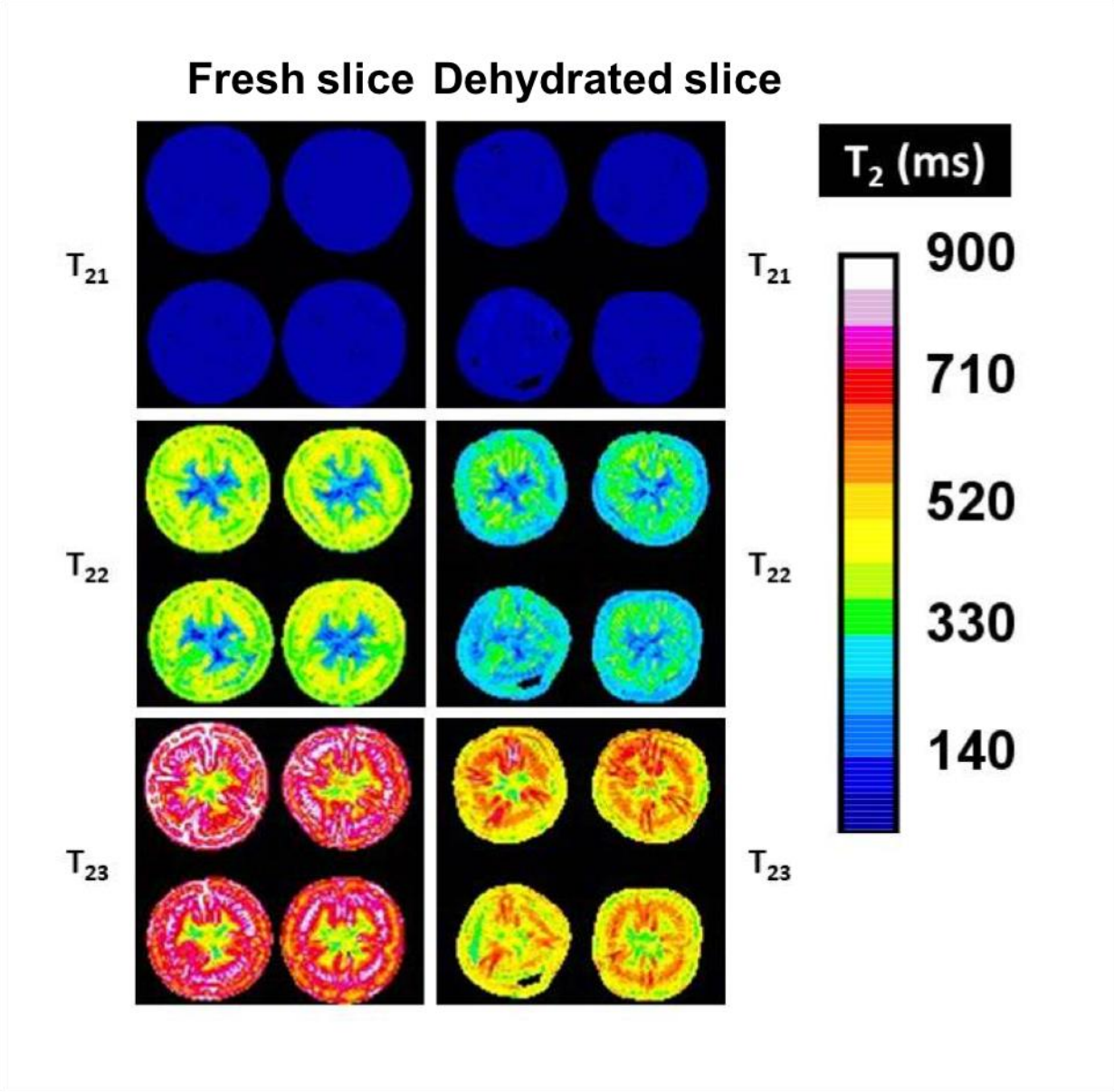
Fresh slice
Dehydrated slice
T21
T21
T22
T22
T23
T23
T2 (ms)
900
710
520
330
140

B

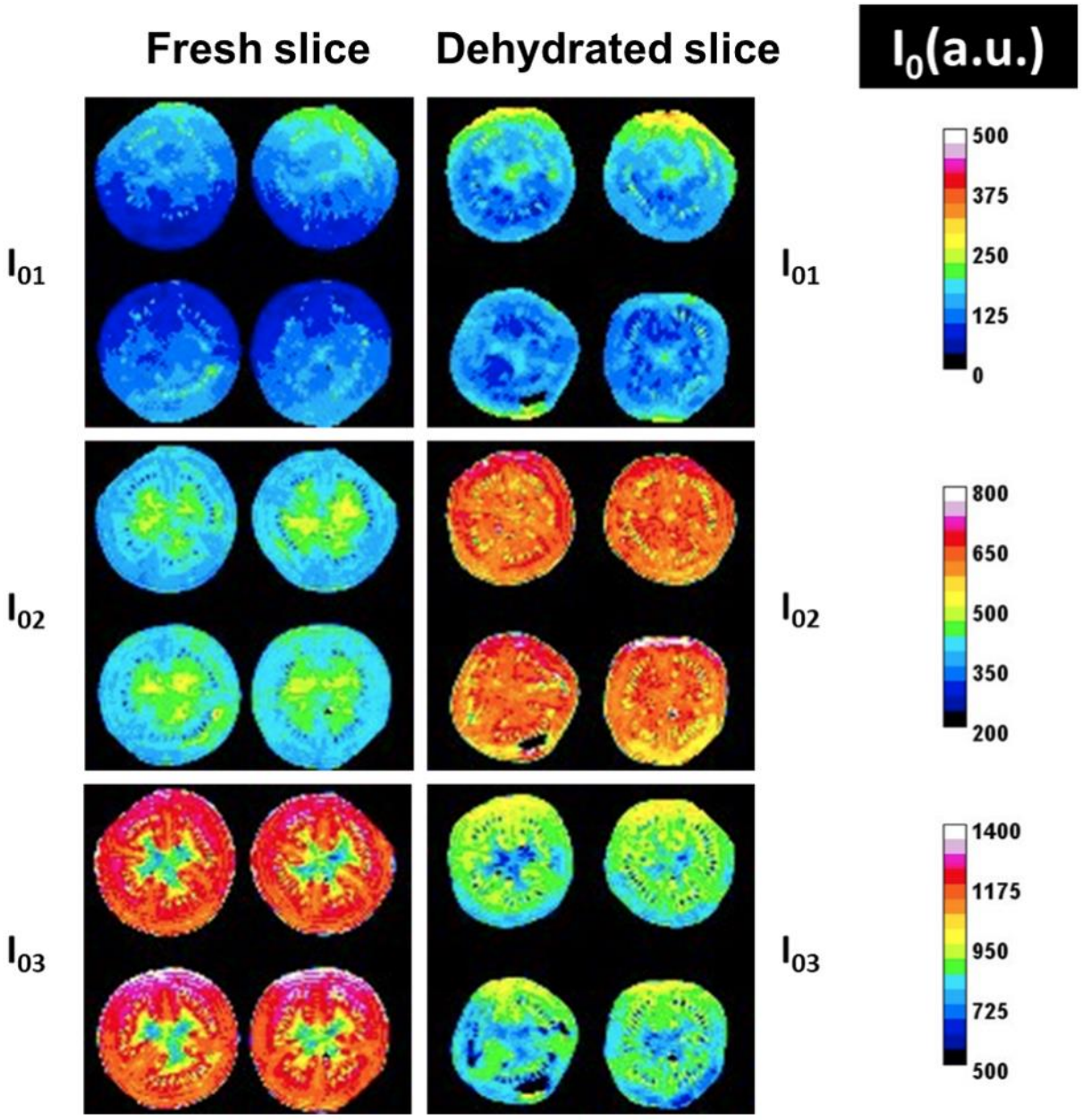

Figure 4: (A) tri-exponential T_2 maps and (B) associated signal intensity maps, before and after dehydration for regime 1-A.

A

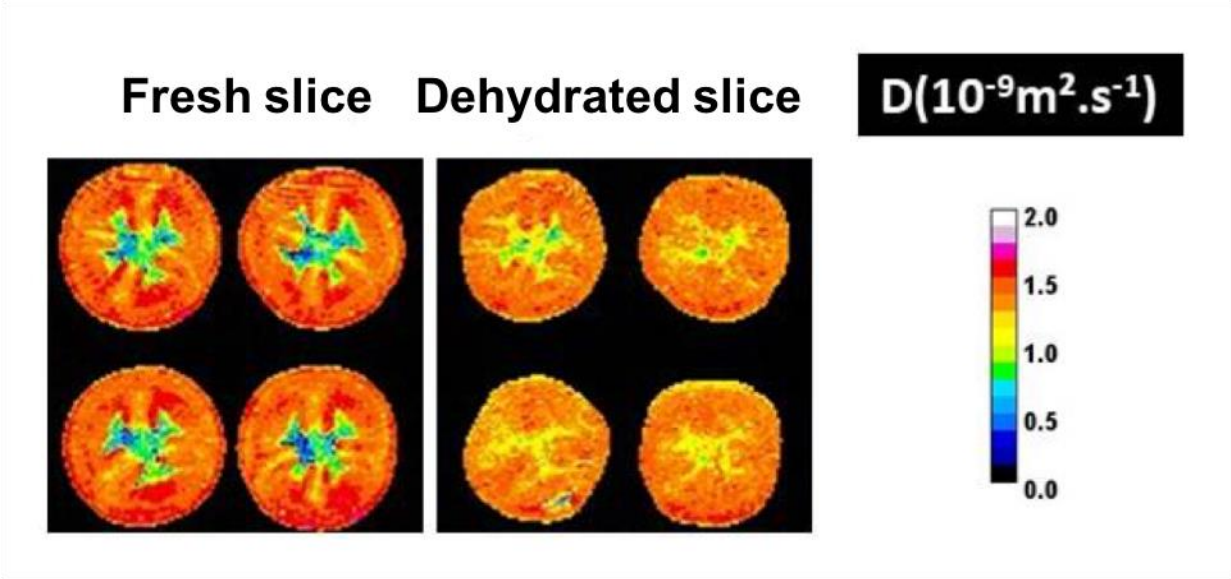

B

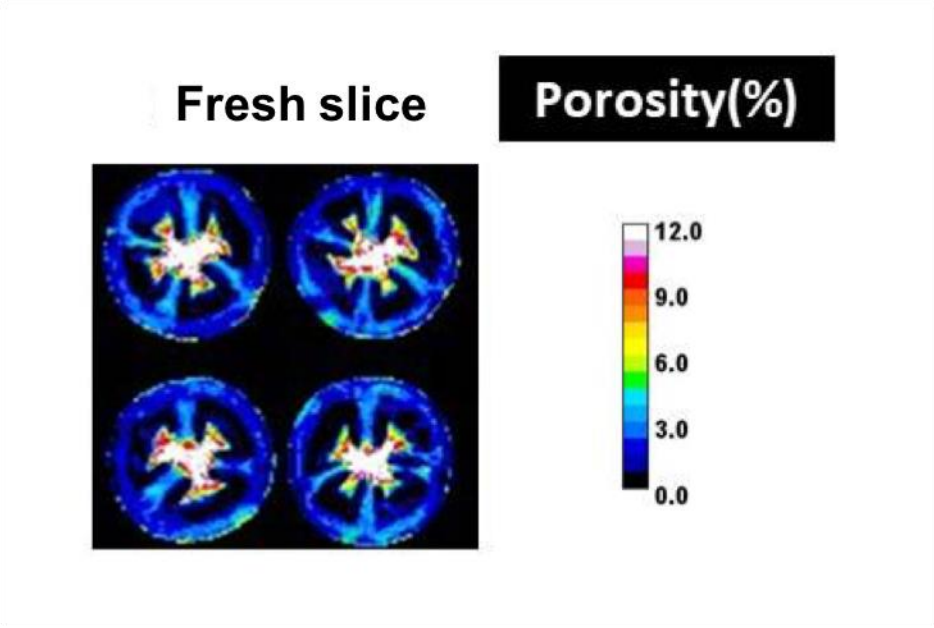

Figure 5: (A) ADC before and after dehydration for regime 1-A. (B) microporosity maps before dehydration for regime 1-A.

A

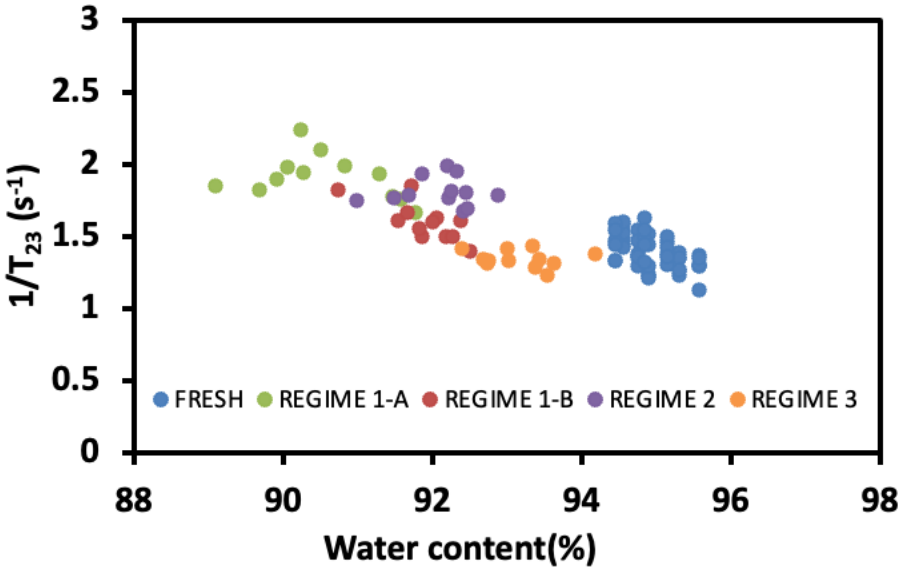

B

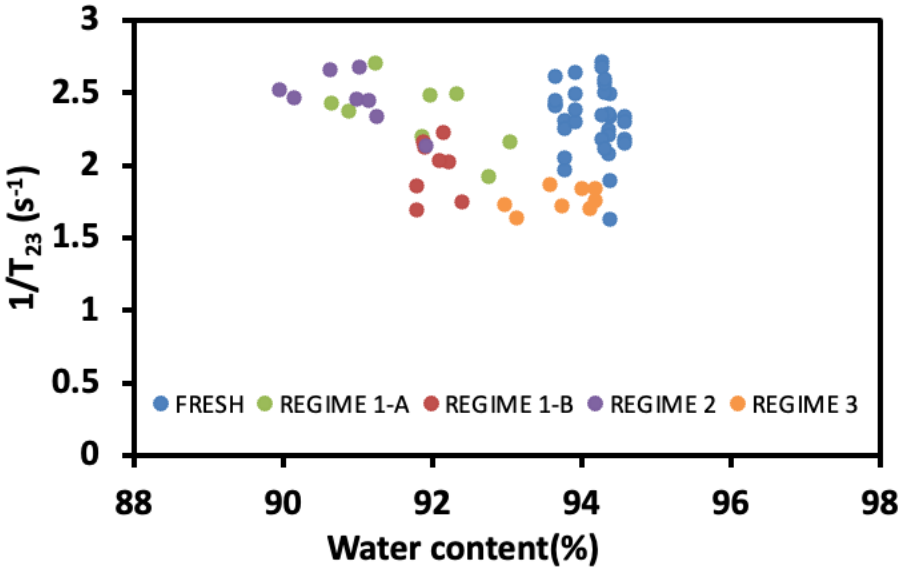

Figure 6 A and B: Relaxation rates of the third transverse relaxation component $1/T_{23}$ as a function of water content for the pericarp (A) and the placenta (B).

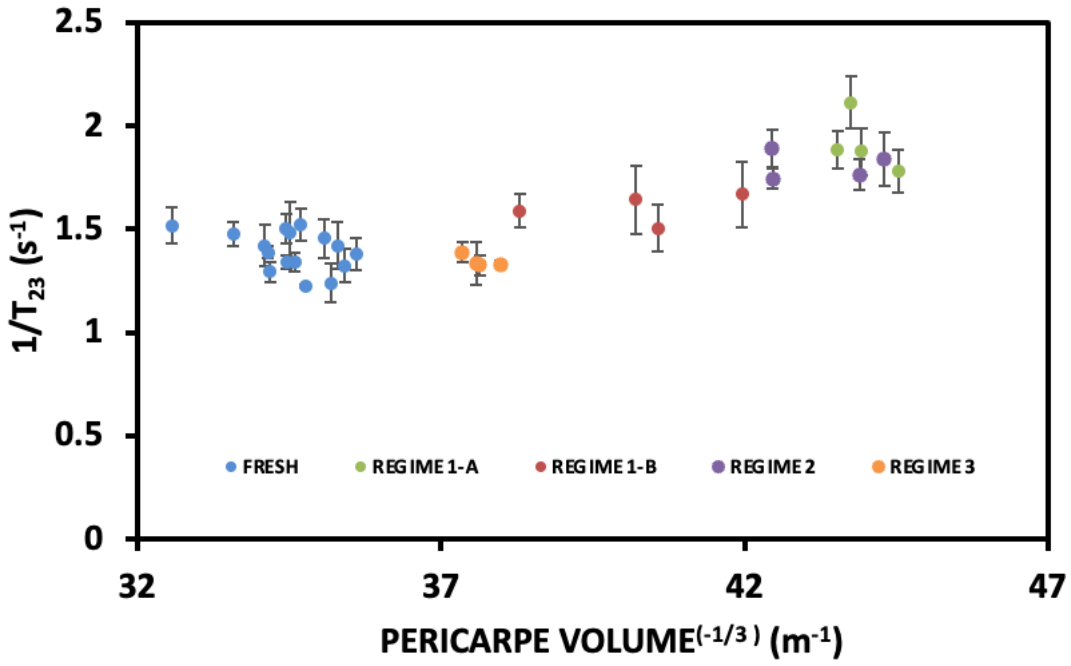

Figure 7: Relaxation rates of the third transverse relaxation component $1/T_{23}$ as a function of the size of the parenchyma cells expressed as the cubic root of the volume of the pericarp. The points correspond to the means and standard deviations calculated for each tomato.

Supplementary Data

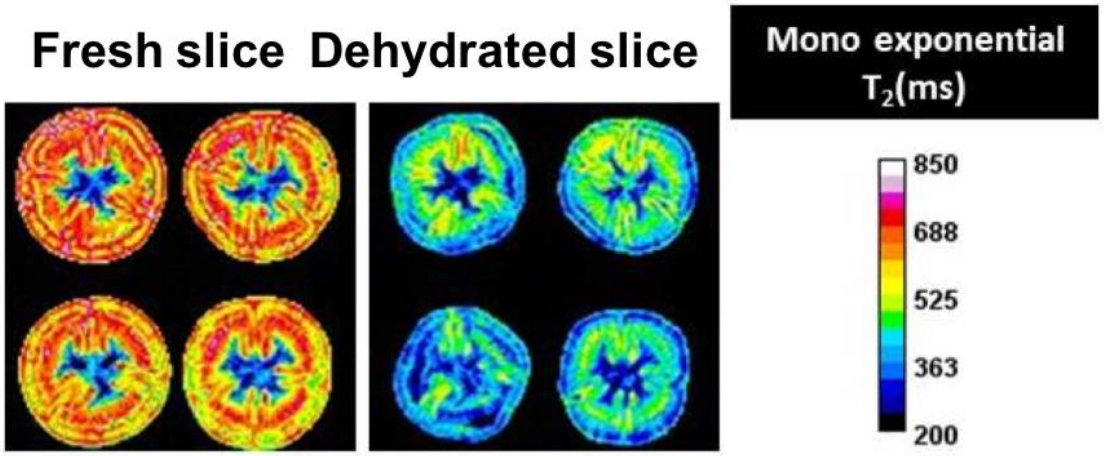

Mono-exponential T_2 maps, before and after dehydration for regime 1-A.